

Noise in Disordered Systems: Higher Order Spectra in Avalanche Models

Amit P. Mehta,^{*} Karin A. Dahmen,[†] M. B. Weissman,[‡] and Tim Wotherspoon

*Department of Physics, University of Illinois at Urbana-Champaign,
1110 West Green Street, Urbana, IL 61801-3080*

(Dated: November 15, 2018)

Abstract

We present a novel analytic calculation of the Haar power spectra, and various higher order spectra, of mean field avalanche models. We also compute these spectra from a simulation of the zero-temperature mean field RFIM and infinite range RFIM model for $d = 3$. We compare the results and obtain novel exponents.

PACS numbers: 64.60.Ht, 75.60.-d, 72.70+em

^{*}apmehta@uiuc.edu

[†]dahmen@uiuc.edu

[‡]mbw@uiuc.edu

Introduction: Certain disordered systems *crackle*, that is when such a system is slowly driven it responds by discrete jumps or avalanches of a broad range of sizes [1]. This crackling is often the result of non-equilibrium collective transport in random media, where the interactions are strong enough that thermal effects are negligible and the system has many interacting degrees of freedom. Such systems include: charge density waves, vortices in type II superconductors, crack propagation, earthquakes, and Barkhausen noise in magnets. In mean field theory the avalanche dynamics of the systems mentioned above are described by Poisson statistics (given by Eq. (1)) at the critical point or critical depinning transition [2, 3].

In our novel mean field analysis we determine the following spectral functions: Haar power spectra, 1.5 spectra, and second spectra for systems that have avalanche dynamics given by Eq. (1). Haar power spectra allow us to obtain a power series in time, $H(t, f_1)$, needed to calculate higher order spectra. Higher order spectra give valuable information about the avalanche dynamics in Barkhausen noise not accessible through ordinary power spectra [4, 5]. Also, higher order spectra have been used to obtain crucial information about a variety of diverse systems such as: metastable states in vortex flow [6], natural auditory signals [7], conductance-noise power fluctuations [8], non-Gaussian $1/f$ noise [9], and spin glasses [10]. While much experimental work has been done studying higher order spectra [4, 5, 6, 7, 8, 9, 10], we present a rigorous mean field treatment that is applicable to a broad range of systems [3]. This analysis is one of a small number of theoretical calculations in higher order noise statistics.

We also compare our general results from mean field theory to a mean field simulation of the $T = 0$ random field Ising model (RFIM) [11], and an analysis of Barkhausen noise obtained from a simulation of the $T = 0$ infinite range RFIM in $d = 3$. We also find novel exponents from our analysis.

Mean Field RFIM: The $T = 0$ mean field RFIM consists of an array of N spins ($s_i = \pm 1$), which may point up ($s_i = +1$) or down ($s_i = -1$). Spins are coupled to all other spins (through a ferromagnetic exchange interaction J), and to an external field $H(t)$ which is increased adiabatically slowly. To model dirt in the material, we assign a random field, h_i , to each spin, chosen from a distribution $P(h_i) = \exp(-h_i^2/2R^2)/\sqrt{2\pi}R$, where R , the disorder, determines the width of the Gaussian probability distribution and therefore gives a measure of the amount of quenched disorder for the system. The Hamiltonian for the system at a time

t is given by: $H = -\sum_i (JM + H(t) + h_i)s_i$, where $M = \frac{1}{N} \sum_j s_j$ is the magnetization of the system. Initially, $H(-\infty) = -\infty$ and all the spins are pointing down. Each spin is always aligned with its local effective field $h_i^{eff} = JM + H(t) + h_i$.

RFIM with Infinite Range Forces in 3D: The $T = 0$ Infinite Range RFIM (IRM) consists of a 3D lattice of N spins, with a Hamiltonian at a time t is given by: $H = \sum_{\langle ij \rangle} -Js_i s_j - \sum_i (H(t) + h_i - J_{inf}M)s_i$, where $J_{inf} > 0$ is the strength of the infinite range demagnetizing field, and $\langle ij \rangle$ stands for nearest neighbor pairs of spins. The local effective field is given by $h_i^{eff} = J \sum_{\langle ij \rangle} s_j + H(t) + h_i - J_{inf}M$.

The addition of a weak $J_{inf} \sim \frac{1}{N}$ to the traditional RFIM causes the system to exhibit self-organized criticality (SOC) [12, 13, 14]. This means that as H is increased the model always operates at the critical depinning point, and no parameters need to be tuned to exhibit critical scaling behavior (except $\frac{dH}{dt} \rightarrow 0$). We limit our analysis to a window of H values where the slope of $M(H)$ is constant and the system displays front propagation behavior. Details of the simulation are given elsewhere [15].

Avalanche Dynamics in the $T = 0$ RFIM: The external field $H(t)$ is adiabatically slowly increased from $-\infty$ until the local field, h_i^{eff} , of any spin s_i changes sign, causing the spin to flip [2, 16]. It takes some microscopic time Δt for a spin to flip. The spin flip changes the local field of the coupled spins and may cause them to flip as well, etc. This *avalanche* process continues until no more spin flips are triggered. Each step of the avalanche, that is each Δt , in which a set of spins simultaneously flip, is called a *shell*. The number of spins that flip in a shell is directly proportional to the voltage $V(t)$ during the interval Δt that an experimentalist would measure in a pick-up coil wound around the sample. In our simulations we denote the number of spins flipped in a shell at a time t by $n_t (= V(t))$. The first shell of an avalanche (one spin flip) is triggered by the external field $H(t)$, while each subsequent shell within the avalanche is triggered only by the previous shell, since $H(t)$ is kept constant while the avalanche is propagating. $H(t)$ is only increased when the current avalanche has Stopped, and is increased only until the next avalanche is triggered (i.e. $\frac{dH}{dt} \rightarrow 0$). The number of shells in an avalanche times Δt defines the *pulse duration*, T , or the time it took for the entire avalanche to flip. The time series of n_t values for many successive avalanches creates a Barkhausen train.

Poisson Distribution: In order to calculate the Haar power spectrum and higher order spectra we first need the probability distribution for an (infinite) avalanche at criticality in

the class of mean field avalanche models we are studying [3], which is given by the following Poisson distribution [2, 3]:

$$P(n_0 = 1, n_1, n_2, \dots, n_\infty) = \frac{1}{en_1!} \prod_{t=2}^{\infty} \frac{e^{-n_{t-1}} n_{t-1}^{n_t}}{n_t!} \quad (1)$$

An avalanche begins with a discrete jump of unit magnitude, so we have $n_0 = 1$, in the context of Barkhausen noise each avalanche begins with one spin flip. Now $\langle \dots \rangle \equiv \sum_{\{n_1, \dots, n_\infty\}} \dots P(n_1, \dots, n_\infty)$ represents the average over Eq. (1). Using Eq. (1) we determine the 2-pt, 3-pt, and 4-pt time-time correlation functions, that allow us to analytically calculate the Haar spectra and higher order spectra. Details are left for a long paper.

Haar Series and Haar Transform: The Haar transform, $H(t, f_1)$, a simple wavelet transformation, is the square wave equivalent of the Fourier transform; where $H(t, f_1)$ is the absolute square of the time integral over a period (of duration $\frac{1}{f_1}$) of the square wave times a section of the train centered around t [4]. The Haar transform affords us the needed time resolution at the expense of frequency resolution that is extraneous to our purpose, since we are interested in studying how the power contribution at a given frequency f_1 changes in time.

We first determine the Haar power series for a single large avalanche of duration T (in the limit that $T \rightarrow \infty$) using the 2-pt correlation function. We obtain the following exact result: $H(t, f_1) = \frac{1}{12}(2\frac{(\Delta t)^2}{f_1} + \frac{1}{f_1^2})$ Moreover, to find the Haar power we sum our result over the whole avalanche to obtain:

$$S_H(f_1) \equiv \frac{1}{T} \sum_{t=1}^{Tf_1} H(t, f_1) = \frac{1}{12}(2(\Delta t)^2 + \frac{1}{f_1^2}) \quad (2)$$

This result differs from the Fourier power, $S_F(f_1) = \frac{1}{f_1^2}$ [2], by an additive constant and a constant factor. This is an artifact of doing a discrete transform. We sum from $t = 1$ to Tf_1 (not to T) since we are summing over Haar wavelets of duration $\frac{1}{f_1}$. We reaffirm the above result (Eq. (2)) through a mean field simulation.

1.5 Spectra and Second Spectra: The 1.5 spectra, and second spectra are defined below:

$$S_{1.5}(f_2, f_1) = \frac{\langle F_t\{v(t, f_1)\} F_t^*\{H(t, f_1)\} \rangle}{\sum_t H(t, f_1)} \quad (3)$$

$$S_2(f_2, f_1) = \frac{\langle F_t\{H(t, f_1)\} F_t^*\{H(t, f_1)\} \rangle}{(\sum_t H(t, f_1))^2} \quad (4)$$

where $v(t, f_1)$ is the sum of n_i around time t over a duration $\frac{1}{f_1}$, and f_2 is the frequency conjugate to t . Also, $F_t\{\dots\}$ is the discrete Fourier transform (FT) with respect to t , and $\sum_t \equiv \sum_{t=1}^{Tf_1}$.

To calculate Eq. (3-4) we first write the product of FTs as the FT of a convolution. This leaves us with the following quantities: $\langle v(t, f_1)H(t + \theta, f_1) \rangle$, and $\langle H(t, f_1)H(t + \theta, f_1) \rangle$ where θ is the convolution variable. These quantities may then be rewritten as sums of 3-pt or 4-pt correlation functions, and subsequently evaluated. We obtain the following results:

$$\Gamma_{1.5}(f_1) \equiv \sum_{t=1}^{Tf_1} \langle v(t, f_1)H(t, f_1) \rangle \simeq \frac{A_{1.5}}{f_1^{Q_{1.5}}} \quad (5)$$

$$\Gamma_2(f_1) \equiv \sum_{t=1}^{Tf_1} \langle H(t, f_1)H(t, f_1) \rangle \simeq \frac{A_2}{f_1^{Q_2}} \quad (6)$$

$$Re\{S_{1.5}(f_2, f_1)\} = \frac{B_{1.5}}{f_2^{V_{1.5}}} + \Gamma_{1.5}^{(N)}(f_1) \quad (7)$$

$$S_2(f_2, f_1) = \frac{B_2}{f_2^{V_2}} + \Gamma_2^{(N)}(f_1) \quad (8)$$

where $V_{1.5}$, V_2 , $Q_{1.5}$, Q_2 are given in Table I for mean field theory, the mean field simulation, and the IRM. Also, $A_{1.5}$, A_2 , $B_{1.5}$, and B_2 are non-universal constants. Plots of Eqs. (7-8) are given in Figs. (2)-(3).

Now $\Gamma_{1/2}(f_1)$ and $\Gamma_2(f_1)$ are independent of f_2 , and result from the $\theta = 0$ evaluation of $\langle v(t, f_1)H(t + \theta, f_1) \rangle$, and $\langle H(t, f_1)H(t + \theta, f_1) \rangle$ (see Fig. 1). These f_2 independent terms are referred to as the DC background terms [9]. The functions $\Gamma_{1.5}^{(N)}(f_1)$ and $\Gamma_2^{(N)}(f_1)$ are $\Gamma_{1.5}(f_1)$ and $\Gamma_2(f_1)$ normalized by $\sum_t H(t, f_1)$ and $(\sum_t H(t, f_1))^2$, respectively. Consideration of $Im\{S_{1.5}(f_2, f_1)\}$ is left for a long paper.

We have left Eq. (5-8) in terms of general scaling forms since we ascertain that our mean field and IRM simulations obey the same scaling forms only with different exponents and non-universal constants.

Mean Field Simulation: We perform 300 runs of a simulation of the mean field RFIM. We collect data taken from $H \in [0, 0.00125]$ at $R = 0.79788$ ($R_c = 0.79788456$) in systems with $N = 15 \times 10^6$ spins, and $J = 1$. The results of our simulation agree with the scaling forms given in Eq. (5-8) with exponents given by Table I. See Fig. 1-3.

Infinite Range Model Simulation: We perform 60 runs of a 3D simulation of the infinite range RFIM. The data was taken from $H \in [1.25, 1.88]$ (from the slanted part of the hys-

	$V_{1.5}$	V_2	$Q_{1.5}$	Q_2
MFT	2	2	3	5
MF Sim.	1.93 ± 0.10	1.92 ± 0.12	2.95 ± 0.10	4.93 ± 0.12
IRM ($d = 3$)	1.80 ± 0.07	1.80 ± 0.05	2.73 ± 0.06	4.46 ± 0.07

TABLE I: We present the values of the exponents: $V_{1.5}$, V_2 , $Q_{1.5}$, and Q_2 given in Eqs. (5-8) for mean field theory (MFT), mean field simulation (MF Sim.), and the infinite range model (IRM) for $d = 3$. While the exponents values for MFT were determined analytically, the exponents for the MF Sim. and IRM were determined through a non-linear curve fitting of simulation data.

teresis loop) at $R = 2.2$ in system with $N = 400^3$ spins, $J_{inf} = \frac{1}{N}$, and $J = 1$. Again, the results agree with Eq. (5-8) with exponents given in Table I. Refer to Fig. 1-3.

Finite Size Effects: We check finite size effects in our mean field and IRM simulations by looking at higher order spectra for various system sizes. We find that for smaller system sizes the high frequency scaling (and flattening due to the DC background term) is unchanged for second spectra and 1.5 spectra. However, at low frequency the scaling regime of the second spectra and 1.5 spectra flattens (in MF Sim.) or rolls over (in IRM) at frequency $f_1 \simeq \frac{1}{T_{max}}$, where T_{max} is the maximum avalanche duration. T_{max} is system size dependent since $T_{max} \sim L^z$, where $L = N^{1/d}$ ($d = \text{dimension of system}$). For a $N = 400^3$ system we find that $T_{max} \simeq 4300\Delta t$.

Discussion: We first notice that the exponents for our MF simulation are systematically smaller (by an amount of 1% to 4%) than the MFT exponents, since the MF simulation results were obtained from a train of finite avalanches while our MFT calculation was for a single infinite avalanche. The intermittency introduced by a train of finite avalanches apparently lowers the magnitude of the mean field exponents since the intermittency effectively adds white inter-avalanche noise to the intra-avalanche noise seen in the MF calculation.

For the DC components ($\theta = 0$) of the higher order spectra (see Fig. 1) we find excellent agreement between MFT and the MF simulation. In fact the exponents Q_2 and $Q_{1.5}$ are not novel; with the help of [11] we ascertain the following exponent relations: $Q_2 = \frac{5-\tau}{\sigma\nu z} - 2$ and $Q_{1.5} = \frac{1}{\sigma\nu z} + 1$. Using the values given in [17] for τ and $1/\sigma\nu z$ we find exact agreement in MFT: $Q_2 = 5$ and $Q_{1.5} = 3$, and in the IRM in $d = 3$ we find $Q_2 = 4.40 \pm 0.10$ and $Q_{1.5} = 2.72 \pm 0.03$, in close agreement with the table above.

In Fig. (2-3) we present the 1.5 spectra and the second spectra. We determine the high frequency power law exponent for the 1.5 spectra and second spectra given by the exponents $V_{1.5}$ and V_2 respectively (see Table I). Upon subtracting the DC background we find that the second spectra, for different f_1 values, collapses (see Inset of Fig. 3). Since the DC background term is small for the 1.5 spectra, we find a collapse without subtracting the DC background.

The weak dependence of 1.5 spectra on f_1 and the strong fall off of the second spectra at high frequency in both the MF Sim. and IRM suggests that the high frequency noise comes from the fine structure of large avalanches ($T_a \gg 1/f_1$, T_a is the avalanche duration) and not small individual pulses ($T_a \simeq 1/f_1$)[5]. Through simulation we verify this claim in the MF Sim. and IRM. When we subtract all avalanches smaller than $T_{max}/4$ from the Barkhausen train and then determine the second spectra we find no change in V_2 . However, when we subtract all avalanches larger than $T_{max}/4$ from the Barkhausen train, we find that the second spectra flattens and that there is an evident separation between the 1.5 spectra curves (i.e. increased f_1 dependence).

Our study of higher order spectra is a powerful tool to further our understanding of noise in disordered systems. Our mean field results are applicable to a large array of systems, in particular systems discussed in [3]. In a future long paper we plan to include details of all the calculations, and a comparison with experiment results.

Acknowledgments

We would like to thank J. Sethna for helpful discussions, and we thank M. Kuntz and J. Carpenter for providing the front propagation model simulation code. K.D. and A.P.M. acknowledge support from NSF via Grant Nos. DMR 03-25939(ITR), the Materials Computation Center, through NSF Grant No. 03-14279, and IBM which provided the computers that made the simulation work possible. M.B.W. acknowledges support from NSF via Grant No. DMR 02-40644. A.P.M. would also like to acknowledge the support provided by UIUC through a University Fellowship, and K.D. gratefully acknowledges support through an A.P.

Sloan fellowship.

-
- [1] J.P. Sethna, K. A. Dahmen, and C.R. Myers, *Crackling Noise*, Nature **410**, 242 (2001).
 - [2] Matthew C. Kuntz, and James P. Sethna, Phys. Rev. B **62**, 11699 (2000).
 - [3] D.S. Fisher, Phys. Reports **301**, 113 (1998).
 - [4] K.P. O'Brien and M.B. Weissman, Phys. Rev. E **50**(5), 3446 (1994); K.P. O'Brien and M.B. Weissman, Phys. Rev. A **46**(8), R4475 (1992)
 - [5] J.R. Petta, M.B. Weissman, and G. Durin, Phys. Rev. E **57**(6), 6363 (1998).
 - [6] R.D. Merithew, M.W. Rabin, M.B. Weissman, M.J. Higgins, and S. Bhattacharya, Phys. Rev. Lett. **77**(15), 3197 (1996).
 - [7] M.G.A. Thomson, Phys. Rev. Lett. **86**(13), 2901 (2001).
 - [8] C.E. Parman, N.E. Israeloff, and J. Kakalios, Phys. Rev. Lett. **69**(7), 1097 (1992).
 - [9] G.T. Seidler, and S.A. Solin, Phys. Rev. B **53**(15), 9753 (1996).
 - [10] M.B. Weissman, Annu. Rev. Mater. Sci. **26**, 395 (1996).
 - [11] K. A. Dahmen, *Hysteresis, Avalanches, and Disorder Induced Critical Scaling: A Renormalization Group Approach*, Ph.D. Thesis, Cornell University (May 1995).
 - [12] J.S. Urbach, R.C. Madison, and J.T. Markert, Phys. Rev. Lett. **75**(2), 276 (1995).
 - [13] O. Narayan, Phys. Rev. Lett. **77**(18), 3855 (1996).
 - [14] S. Zapperi, P. Cizeau, G. Durin, and H.E. Stanley, Phys. Rev. B **58**(10), 6353 (1998).
 - [15] Matthew C. Kuntz, Olga Perković, Karin A. Dahmen, Bruce W. Roberts, and James P. Sethna, *Comput. Sci. Eng.* **1**, 73 (1999).
 - [16] James P. Sethna, Olga Perković, and Karin A. Dahmen, preprint (1997), Los Alamos Nat'l Laboratory Archive, <http://xxx.lanl.gov/abs/cond-mat/9704059>.
 - [17] Amit P. Mehta, Andrea C. Mills, Karin A. Dahmen, and James P. Sethna, Phys. Rev. E **65**, 46139 (2002).

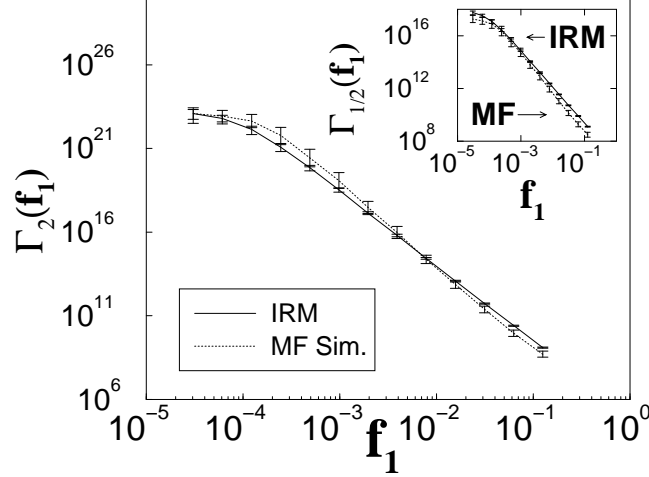


FIG. 1: We present $\Gamma_2(N)$ in the MF Sim. and in the IRM. For high frequency $\Gamma_2(N) \sim f_1^{-Q_2}$. Inset: $\Gamma_{1/2}(N)$ for the MF and the IRM. For high frequency $\Gamma_{1/2}(N) \sim f_1^{-Q_{1.5}}$, see Table I.

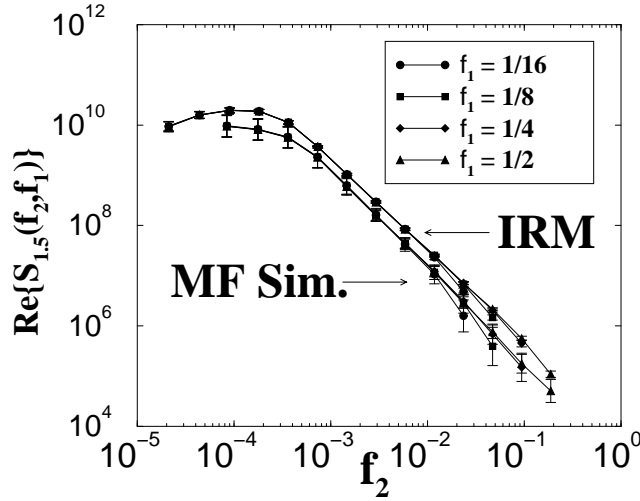


FIG. 2: We present the $\text{Re}\{S_{1.5}(f_2, f_1)\}$ in the MF Sim. and in the IRM. At high frequency $\text{Re}\{S_{1.5}(f_2, f_1)\} \sim f_2^{-V_{1.5}}$ (go to Table I). There is no visible flattening present due to $\Gamma_{1.5}^{(N)}(f_1)$ ($\theta = 0$) term, since the magnitude of this term is small relative to the f_2 dependent term.

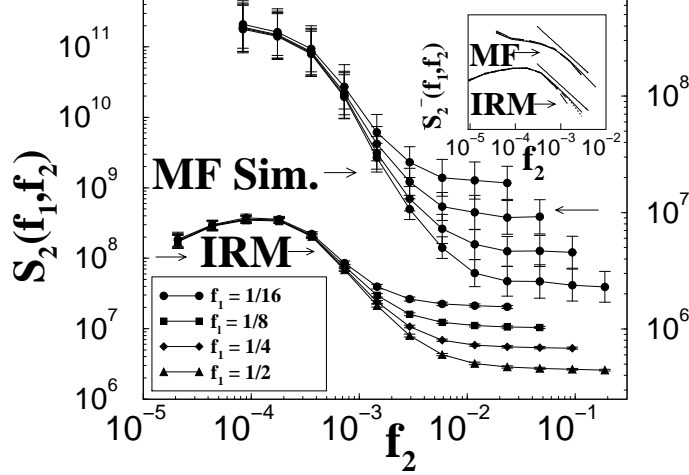


FIG. 3: We present the $S_2(f_2, f_1)$ in the MF Sim. and IRM. Notice the flattening due to the $\Gamma_2^{(N)}(f_1)$ ($\theta = 0$) term. At high frequency $S_2(f_2, f_1) \sim f_2^{-V_2} +$ (DC background). We use a non-linear curve fit of the form: $A0 * x^{-A1} + A2$ to determine the V_2 exponent given in Table I. Inset: $S_2^-(f_2, f_1)$ is the second spectra in the MF Sim. and the IRM with the theoretical DC background term subtracted. The bold lines adjacent to the MF curve and the IRM curve have an exponent of -2 and -1.8, respectively. Please note that these curves (in the inset) do not show the full range of data points, and are simply presented to illustrate that we have a power law in the absence of the DC background term.